Triplet Topology of Self-Assembled Zinc Porphyrin−Pyridylfullerene Complex†

Ayelet Regev,‡ Tamar Galili,‡ Haim Levanon,*,‡ and David I. Schuster*,§

Department of Physical Chemistry and the Farkas Center for Light-Induced Processes, The Hebrew University of Jerusalem, Jerusalem 91904, Israel, and Department of Chemistry, New York University, New York, New York 10003

Received: March 7, 2006

This work extends a recent EPR study on light-driven electron and energy transfer in a self-assembled zinc porphyrin−pyridylfullerene (ZnP−PyrF) complex.[1] We report on a triplet line shape analysis of the photoexcited PyrF monomer and the ZnP−PyrF complex dissolved in isotropic and anisotropic matrixes of different polarity, namely, toluene, tetrahydrofuran (THF), and the nematic liquid crystals (LCs), E-7 and ZLI-4389. The line shape of the unbound ^{3}*PyrF obtained in both isotropic matrixes exhibits triplet parameters similar to those obtained for other monoadducts of C_{60} under similar experimental conditions. On the other hand, ^{3}*PyrF oriented in the LCs shows a complicated line shape, which is attributed to two conformers: (a) an axial dominant (85%) configuration characterized by triplet parameters, similar to those obtained in the isotropic matrixes and (b) a bent configuration associated with spin density localized about the poles accompanied by sign reversal of the ZFS parameter *D* of the ^{3}*C_{60} moiety. Further, since in both LCs the ZnP−PyrF complex mainly exhibits a conformation with axial symmetry, the differences between the electron and the energy transfer routes in each LC are attributed to their different polarity. This study reflects the strength of LC matrixes to serve as a topological tool, enabling us to determine the conformers' distribution and to differentiate between electron and energy transfer routes.

Introduction

Exceptional properties of fullerenes make them potentially useful in basic and practical applications. Recently, the synthesis of functionalized fullerene derivatives has become a flourishing branch in material science.[2−5] Functionalized fullerenes, which retain the original properties of pristine C_{60}, offer the possibility of covalently linking C_{60} to different groups, thus combining the outstanding properties of fullerenes with those of other suitable molecules.

In terms of modern photochemistry, efforts in mimicking primary photosynthesis and related biological systems resulted in the design of many biomimetic systems, using fullerene as an acceptor coupled via covalent linkage to a donor.[6] A different approach to organize the donor−acceptor couples is self-assembling of the individual molecules, linked by weak intermolecular interactions such as coordinative linkage with metal ions.[7−12] By this method of molecular recognition, it is possible to control the assembly of structurally sophisticated species since reactions of functionalized fullerenes are site-selective.

Recently, we have reported on light-driven processes taking place in the self-assembled, via axial coordination, zinc porphyrin−pyridylfullerene (ZnP−PyrF) complex (**2** in Scheme 1) as studied by time-resolved electron paramagnetic resonance (TREPR) spectroscopy.[1] It was shown that the photoexcitation of the donor part, ZnP, results in competitive energy transfer (EnT) and/or electron transfer (ET) routes to the acceptor, PyrF.

SCHEME 1

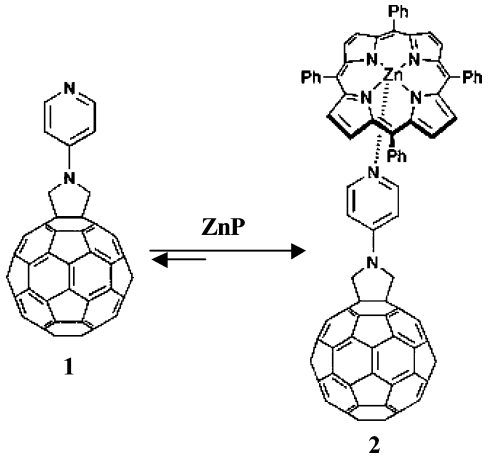

The present paper is focused on the photoinduced triplet state of PyrF in its monomeric form, using pristine C_{60} as a reference, and in the axial coordinatively linked ZnP−PyrF complex. It is well-established that the analysis of the TREPR spectra provides us with a number of parameters related to the detailed structure of the molecules involved in the photodriven processes and their interaction with the environment. We shall show that TREPR is capable of determining the molecular conformational changes and distorted geometries of the self-assembled complex, the solvent effects, and the mutual orientation between the interacting chromophores. In addition, the analysis enables us to distinguish between intramolecular EnT as taking place in the singlet or triplet manifolds. Moreover, temperature dependence of the triplet line shape reveals the molecular dynamic behavior. The present work will cover all relevant points outlined previously.

† Part of the "Chava Lifshitz Memorial Issue".

* Corresponding authors. (H.L.) Tel.: +972-2-658-5544; fax: +972-2-651-8383; e-mail: levanon@chem.ch.huji.ac.il. (D.S.) Tel.: +1-212-998-8447; fax: +1-212-260-7905.

‡ The Hebrew University of Jerusalem.

§ New York University.

10.1021/jp0613992 CCC: $33.50
Published on Web 04/21/2006

Experimental Procedures

The schematic presentation of the pyridylfullerene ligand **1** (PyrF) and zinc tetraphenylporphyrin−pyridylfullerene complex **2** (ZnP−PyrF) is shown in Scheme 1.

Their synthesis and photophysical properties are described elsewhere.[13] Continuous-wave X-band (9.5 GHz) TREPR studies of the photoexcited triplet states of the PyrF monomer **1** and ZnP−PyrF complex **2** were carried out on a Bruker ESP-380 spectrometer with the field modulation disconnected, where the temperature was maintained by variable-temperature nitrogen flow Dewar in the X-band EPR resonator.[14] The TREPR measurements were performed in the isotropic matrixes, namely, toluene and tetrahydrofuran (THF) (Merck Ltd.) and anisotropic nematic liquid crystals (LCs) E-7 and ZLI-4389 (ZLI) (Merck Ltd.), in which the chromophores could be partially oriented. As was described in detail elsewhere,[1] toluene was dried over molecular sieves, and THF was distilled from a sodium and benzophenone solution. The two solvents of each set were chosen due to the difference in their dielectric constants to elucidate the influence of the environment on the EnT and ET branching routes taking place in complex **2**: $\epsilon_{toluene} = 2.38$; $\epsilon_{THF} = 7.58$;[15] $\epsilon_{E-7} = 19.0$; and $\epsilon_{ZLI-4389} = 56.0$.[16] EPR samples (∼0.5 mM) were prepared in 4 mm OD Pyrex tubes and degassed by several freeze−pump−thaw cycles on a vacuum line.

TREPR experiments were carried out over a broad range of temperatures according to the solvent phase diagram

$$\text{toluene: glass} \xrightarrow{117\ \text{K}} \text{amorphous} \xrightarrow{178K} \text{liquid}$$

$$\text{THF: glass} \xrightarrow{164.5\ \text{K}} \text{liquid}$$

$$\text{E-7: crystalline} \xrightarrow{210\ \text{K}} \text{soft crystalline} \xrightarrow{263\ \text{K}} \text{nematic} \xrightarrow{333\ \text{K}} \text{isotropic}$$

$$\text{ZLI-4389: crystalline} \xrightarrow{250\ \text{K}} \text{soft crystalline} \xrightarrow{253\ \text{K}} \text{nematic} \xrightarrow{335\ \text{K}} \text{isotropic}$$

The samples were photoexcited at 532 nm (∼10 mJ/pulse at a repetition rate of 10 Hz) by an OPO laser (Continuum Panther SLII-10) pumped by a third harmonic of a Nd:Yag laser (Continuum Surelite II-10). At this wavelength, the laser pulse mainly excited the donor part, ZnP, since $\epsilon_{532} = \sim 5 \times 10^3\ M^{-1}\ cm^{-1}$ for ZnP[17] and $\sim 0.9 \times 10^3\ M^{-1}\ cm^{-1}$ for PyrF.[18] All experimental spectra were taken 0.7 μs after the laser excitation pulse. In LC matrixes, two distinct orientations of the samples with respect to the magnetic field, B, were studied, namely, $L||B$ and $L\perp B$, where L is the LC director.[19] The initial alignment of the sample is $L||B$, and the $L\perp B$ orientation is obtained by rotating the sample in the microwave cavity by $\pi/2$ about an axis perpendicular to B. In the fluid phases (soft crystalline and nematic), where molecular motion is allowed, only the $L||B$ orientation is maintained. For comparison, the control experiments were carried out also on the pristine C_{60} and on the 1:1 mixture of ZnP and the pristine C_{60}. Line shape analysis of TREPR spectra of photoexcited triplets, oriented in isotropic and anisotropic matrixes, is described in detail elsewhere.[20]

Results and Discussion

As was mentioned previously, we recently reported on the assignment of ET and EnT routes, taking place in the ZnP−PyrF complex, **2**, in different matrixes at different temperatures.[1]

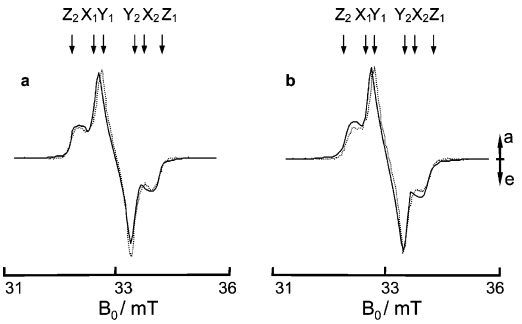

Figure 1. TREPR spectra, $\chi''(B_0)$, of a PyrF monomer dissolved in toluene (dotted line): (a) at 130 K and (b) at 178 Kbb4. The superimposed solid lines are a result of the triplet line shape simulation with parameters in Table 1.

Particularly, the EnT process from the photoexcited donor, ZnP, to the acceptor, PyrF, was determined as taking place in the singlet manifold: ^{1}*ZnP−PyrF → ZnP−^{1}*PyrF. These conclusions were based upon experimental observations from which the energy level diagrams were derived. Nevertheless, only by thorough triplet line shape analysis of the photoexcited monomer PyrF and ZnP−PyrF, one may decide between the two pathways, triplet−triplet EnT: ^{3}*ZnP−PyrF → ZnP−^{3}*PyrF or back ET (BET): ZnP•$^+$−PyrF•$^-$ → ZnP−^{3}*PyrF.[1] Furthermore, one should consider the triplet dynamics in terms of the existence of several conformers as previously suggested by molecular modeling.[21] An additional aspect of the triplet line shape analysis is to compare two different LCs of different polarities versus the isotropic matrixes, toluene and THF.

Before discussing the results, we present relevant findings previously reported. The TREPR spectra of the pristine ^{3}*C_{60} were characterized with the zero field splitting (ZFS) parameters $D \sim -0.0114\ cm^{-1}$ and $|E| \sim 0.0007\ cm^{-1}$.[22−29] It was also shown that the spectra of ^{3}*C_{60} reveal molecular motion in frozen matrixes of toluene and LC, even at temperatures as low as 8 K. In particular, the rotational rate was found to increase continuously between 8 and 298 K in the LC matrix, while the dynamics in toluene was in close correlation with the phase diagram of the solvent.[24] Quantitatively, the spectra observed in the solid and amorphous phases were best described via interconversion between distorted Jahn−Teller configurations. In the isotropic liquid phases (high temperatures), a fast rotating triplet at thermal equilibrium was found to be the origin of the narrow triplet EPR spectrum.[24,25] A W-band ENDOR study of frozen solutions of C_{60} has proven that $D < 0$, with the equator atoms and their adjacent atoms possessing ∼98% of the spin density of the ^{3}*C_{60}.[29−31] Spin localization on the fullerene belt has been verified by calculations of the triplet wave functions.[32,33] For C_{70}, the experimental spin density distribution was found to be displaced toward the poles, resulting in $D > 0$.[33] The magnitude of D was found to be extremely sensitive to the spin density distribution.[33]

Recently, the properties of the photoexcited triplet state of some mono- and bis-adducts of C_{60} were studied by TREPR.[34−38] It was found that the spin distribution varies only slightly upon addition of adducts, their chemical nature, and position. On the other hand, a larger deviation of D relative to that of the pristine C_{60} was found only in more strained structures.[34−36,39] In addition, chemical bonding destroys the high electronic degeneracy and reduces the influence of a pseudorotation and the dynamic Jahn−Teller effect. Thus, for mono- and bis-adducts, the spectral line shape does not change significantly with temperature. Studies of radical anions of fulleropyrrolidins and photoexcited fullerenes linked to a radical probe (e.g., TEMPO)

TABLE 1: Triplet Parameters of PyrF Monomer in Toluene, ZnP−PyrF Complex, and *N*-Methylfulleropyrrolidine[46]

species	T^a	D^b	E^b	$A_x/A_y/A_z$	$1/T_2x^c,1/T_2y^c,1/T_2z^c$
PyrF (Bb1gf)	130	−91	8	0.2:1.0:0.0	1.0,0.5,1.0
PyrF (Bb4gf)	178	−88	8	0.2:1.0:0.0	1.0,0.5,1.0
ZnP−PyrF	130	−91	12	0.1:1.0:0.0	1.0,0.5,1.5
ZnP−PyrF	178	−88	11	0.1:1.0:0.0	1.0,0.5,1.0
N-methylfulleropyrrolidine[46]		−90	14	0.85:1.0:0.3	

[a] K. [b] $\times 10^4$ cm^{-1}. [c] mT.

show that as in the case of a pristine C_{60}, the maxima of the spin density are also localized on the equatorial belt of the fullerene sphere.[40−45] These results are in line with our findings presented next.

Isotropic Matrixes: PyrF Monomer. In Figure 1, we show the TREPR spectra of the PyrF monomer dissolved in toluene in the glass phase and about the glass−liquid transition. The spectra superimposed on the experimental results are line shape simulations with triplet parameters reminiscent of other monoadducts of fullerene in toluene (Table 1).[34,36,46] Similar to the other monoadduct, the spectra in Figure 1 do not reveal the pseudodynamic features between Jahn−Teller configurations typical of the highly symmetrical pristine configuration[3] at these temperatures. In addition, the smaller *D* values, as compared to ^{3}*C_{60}, are in line with the electron withdrawing property of the pyrrolidine group and with the values found elsewhere in similar monoadducts. [46] The *E* values of the PyrF monomer (Table 1) are only slightly larger than those obtained for ^{3}*C_{60}, suggesting a somewhat larger deviation from an axial symmetry. Above the glass−liquid transition, at 200 K, only a thermal (absorptive) broad and asymmetric line is detected (not shown). Similar features were observed in the TREPR spectra of the monomer dissolved in frozen THF.

LC Matrixes: PyrF Monomer. Figure 2 shows the spectra of the PyrF monomer, oriented in E-7 and taken at temperatures between 130 and 280 K, which cover the crystalline, soft crystalline, and nematic phases. Similar spectra were detected in ZLI (not shown). The spectra taken at the $L||B$ and $L\perp B$ configurations are unique and do not obey the well-known relationship between the parallel and the perpendicular spectra. These spectra will be discussed in terms of two triplet systems, namely, $X^IY^IZ^I$ and $X^{II}Y^{II}Z^{II}$. In more detail, the spectra obtained at the $L\perp B$ configuration, in the crystalline and soft crystalline phases, are similar to those obtained in toluene at these temperatures showing contributions from all canonical orientations (cf. Figure 1). Moreover, these spectra differ from those obtained at the $L||B$ configuration. At temperatures up to 210 K, where the parallel and perpendicular spectra can be differentiated, the $L||B$ spectra exhibit a much lower *S*/*N* ratio, with a stronger emission (low field)/absorption (high field) at the X^{II} canonical orientation and the appearance of additional outer lines at Z^{II}. This behavior becomes more apparent at higher temperatures $\geq$220 K, where only the parallel spectra can be detected. Further, at 280 K, a polarization flip was observed in the center at the Y^I canonical orientation (Figure 2).

The experimental spectra (dotted lines) were recorded 0.7 μs after the laser pulse. The smooth solid lines superimposed on the experimental spectra are results of the line shape simulations of the ^{3}*PyrF monomer. The simulations were carried out by taking into account two contributions: (a) a main contribution ($X^IY^IZ^I$ system) characterized by ZFS parameters typical of either pristine ^{3}*C_{60}[22−28] or its monoadducts at above 100 K,[34,36,46] with a triplet of nearly spherical symmetry. This main contribution (~85%) is temperature dependent as reflected by the changes in the relative population rates and with a conspicuous effect of polarization inversion due to spin dynamics (cf. Figure 2 and Table 2). (b) A minor contribution ($X^{II}Y^{II}Z^{II}$ system), which is temperature independent over the entire experimental temperature range, 130−280 K. This contribution (~15%) is characterized by the ZFS parameters of pristine C_{60} at 5 K but with opposite polarization indicative of either sign reversal of the ZFS parameter *D* or selective population of the Z^{II} canonical orientation (Table 2). Sign reversal of *D*, suggested for the $X^{II}Y^{II}Z^{II}$ system (minor contribution), was already observed in other adducts of ^{3}*C_{60}, where the triplet wave function was confined close to the poles.[46,47] The large *D* value as compared to that of ^{3}*C_{60} and its adducts at these temperatures is in line with localization of the spin density in the poles and hence with the sign reversal. However, there is no evidence for photofragments to generate constituents with large *D* values, especially as we did not notice any irradiation damage of the samples. Thus, as will be discussed next, we attribute these values to a different spin distribution. The minor contribution is orientation dependent and is clearly represented by the outmost Z^{II} and inner X^{II} lines (Figure 2). The Z^{II} lines appear

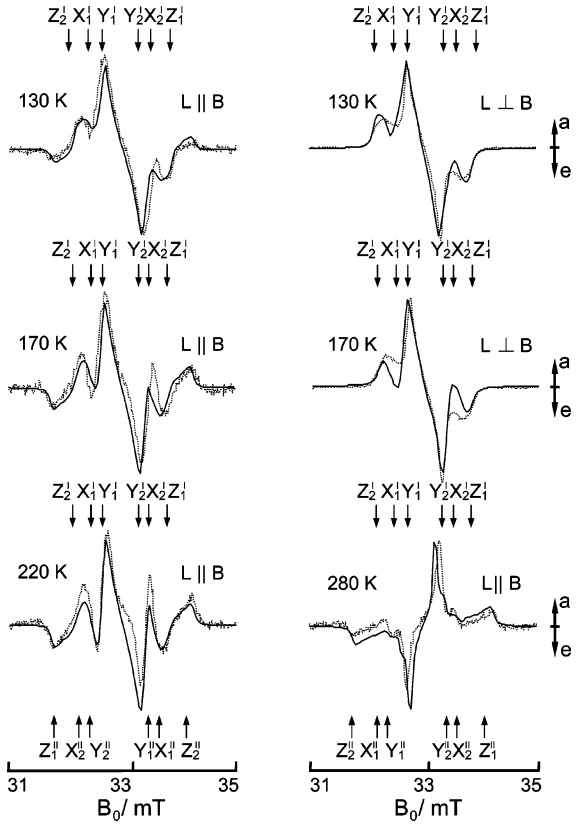

Figure 2. TREPR spectra ($\chi''(B_0)$ presentation) of ^{3}*PyrF monomer oriented in E-7, at different temperatures. The smooth solid lines superimposed on the experimental spectra (dotted lines) are results of the line shape simulation. As found by the line shape simulations, the $X^{II}Y^{II}Z^{II}$ system (minor contribution), shown at the bottom, is the same for all spectra, while the $X^IY^IZ^I$ systems (main contribution) are temperature dependent.

TABLE 2: Triplet Parameters of the Main and Minor Contributions of ^{3}*PyrF in LC Matrices at Different Temperatures

species	T^b	D^b	E^c	$A_x/A_y/A_z$	$T_2{}^d$	orientation
Minor ($X^{II}Y^{II}Z^{II}$)	130−280 (C60n, c60m)	+134	7.5	1.0:1.0:0.0	0.5	nematic
Main ($X^IY^IZ^I$)	130 (Bb1gf)	−93	7.5	0.5:1.0:0.0	0.5	isotropic
Main ($X^IY^IZ^I$)	170 (Bb4gf)	−88	5.35	0.2:1.0:0.0	0.7	isotropic
Main ($X^IY^IZ^I$)	220 (Bb6a)	−88	5.35	0.2:1.0:0.35	0.7	isotropic
main[a] ($X^IY^IZ^I$)	280 (Ab10gf)	−88	7.5	0.2:1.0:0.0	0.2	isotropic

[a] At this temperature, the parameters extracted include discrete $\pi/2$ − jumps about the X and Y dipolar axes with a triplet hopping rate $k \sim 1000$ G (2.8 GHz). [b] K. [c] $\times 10^4$ cm^{-1}. [d] mT.

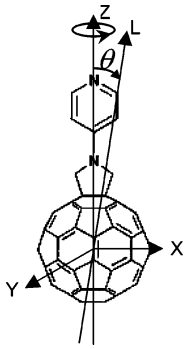

Figure 3. Schematic presentation of the ^{3}*PyrF monomer within the ZFS frame of reference oriented in the nematic LC. The calculated angle θ (8°) is between the LC director, L, and the Z canonical axis. This value was determined from the triplet TREPR spectra via line shape simulations described in detail previously.[17,20]

only in the $L||B$ spectra, which imply also in this case a near pole spin density. This orientation dependence is reversed with respect to most common cases, where the Z lines appear at $L\perp B$.

The two contributions to the triplet spectra of ^{3}*PyrF monomer, in LC matrixes, may be associated with the different models suggested for the complex structure. Although PyrF was designed as an axially symmetric molecule (**1** in Scheme 1), calculations based on molecular dynamics show also a bent geometry.[21] Assigning the bent conformation to the minor contribution may account for both the sign reversal of D and the reversed orientation dependence discussed elsewhere. Associating the main contribution with the axial−symmetric conformer is in line with its high intensity, low-ordered contribution and the relatively stronger $L\perp B$ as compared to the $L||B$ spectra. In particular, the intense $L\perp B$ spectra, together with the X^I,Y^I preferred population rates, suggest that the director is roughly parallel to the Z^I canonical orientation, which for the dominant axial−symmetric configuration should be associated with the main C_2 symmetry axis shown schematically in Figure 3.

LC Matrixes: ZnP−PyrF Complex. The triplet line shape of ZnP−^{3}*PyrF complex in toluene is similar to that obtained for ^{3}*PyrF monomer in the isotropic matrixes at the same conditions and does not provide us with additional information. It should be noted that at later times (e.g., in the time window 3.0−3.5 μs or at higher temperatures (∼200 K), where the spectral features attributed to ZnP−^{3}*PyrF disappear), a signal is observed at $g \sim 2$. We attributed this signal to the radical ion pair, ZnP$\bullet^{+-}$PyrF$\bullet^-$, which arises on excitation of the bound complex.[1] The results confirmed the existence of an equilibrium between association and dissociation of the coordinatively linked complex, which facilitates, after photoexcitation, rapid intramolecular EnT and/or ET, without the indication of intermolecular electron−hole separation.[48] An ordered LC matrix prevents the separation of the complex constituents, thus hindering the creation of long-lived radical pairs even in fluid phases. Therefore, the discussion below is confined to E-7 and ZLI.

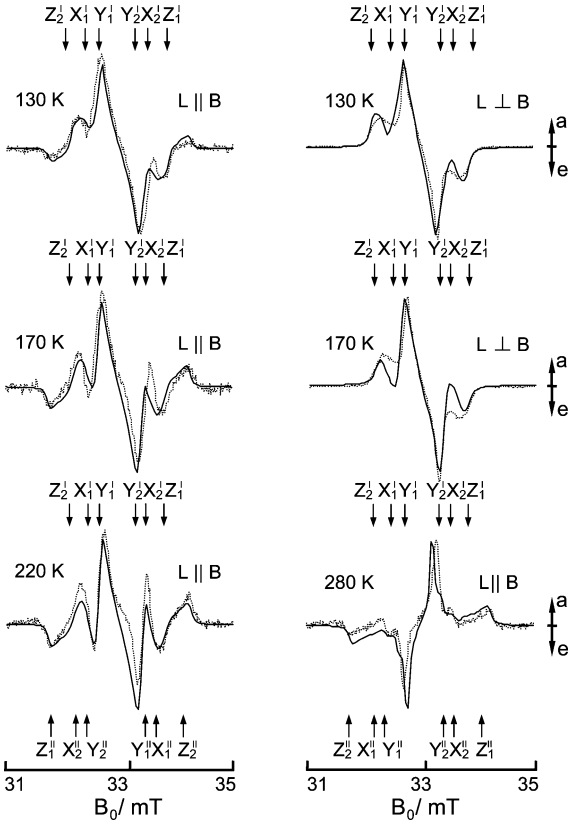

Figure 4. Comparison of the TREPR spectra ($\chi''(B_0)$ presentation) obtained for ^{3}*PyrF (solid) and ZnP−^{3}*PyrF (dotted line) oriented in ZLI at different temperatures.

In Figure 4, we compare the TREPR spectra of ^{3}*PyrF with that of ZnP−^{3}*PyrF, both oriented in ZLI at different temperatures. In the temperature range of 130−170 K, both compounds exhibit the same line shape, attributed to ^{3}*PyrF. Also, the buildup and decay of the magnetization in both cases (not shown) is very similar, implying that both ^{3}*PyrF and ZnP−^{3}*PyrF are generated via similar pathways (i.e., ISC, without an indication of triplet−triplet energy transfer or back electron transfer). Furthermore, the outermost wings, originating from the $X^{II}Y^{II}Z^{II}$ system (bent conformer), are also noticed in the spectrum of ZnP−^{3}*PyrF, especially at higher temperatures near the crystalline → soft crystalline transition. However, these wings are weaker in the complex, indicating that the contribution of the bent conformer to the spectra is smaller than that in the monomer. Also, unlike ^{3}*PyrF, the spectra of ZnP−^{3}*PyrF in the soft crystalline phase do not show the flip of the inner lines (Figure 4, bottom). This behavior implies that although the axial symmetry is maintained, reducing the degrees of freedom in the complex relative to the monomer attenuates the dynamical features of the spectra, as reflected by the absence of the polarization flip. The absence of ^{3}*ZnP−PyrF in the spectra and the different temperature dependence of the spectra

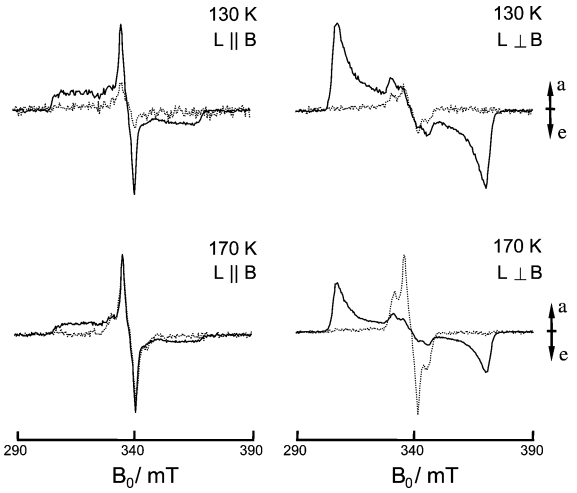

Figure 5. Comparison of the triplet TREPR spectra ($\chi''(B_0)$ presentation) of ZnP−PyrF oriented in E-7 (solid line) and ZLI-4389 (dotted line) at different temperatures. The experimental details, not indicated in the figure, are described in the Experimental Procedures.

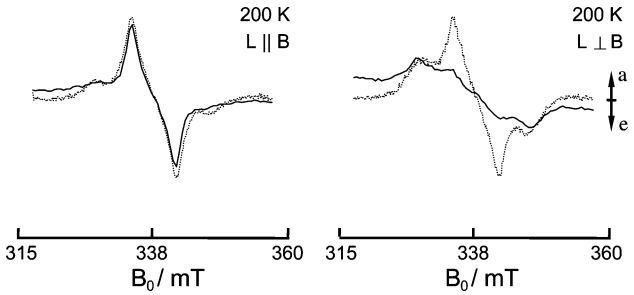

Figure 6. Similar to Figure 5, comparison of the triplet TREPR spectra ($\chi''(B_0)$ presentation) of ZnP−PyrF oriented in E-7 (solid line) and ZLI-4389 (dotted line) but at 200 K and at different magnetic field sweeps. The experimental details, not indicated in the figure, are described in the Experimental Procedures.

(monomer vs complex) may shed some light on the interaction between the complex constituents.

However, in E-7 unlike in ZLI, the spectra at 130−300 K reveal both triplets, ^{3}*ZnP−PyrF and ZnP−^{3}*PyrF, in different fractions (Figures 5 and 6). In the crystalline and soft crystalline phases, the main contribution to the spectra is from ZnP−^{3}*PyrF, while the contribution of ^{3}*ZnP−PyrF increases with temperature, in the nematic phase. Most noticeably, below 260 K, the central part of the $L||B$ spectra (Figure 6, left) is similar to that obtained in ZLI. At the $L\perp B$ configuration below 260 K, or at high temperatures where the ^{3}*ZnP−PyrF is dominant, the similarity between the spectra in E-7 and ZLI is less apparent. Thus, whenever ZnP−^{3}*PyrF dominates the spectra, its features are similar in both E-7 and ZLI and may be analyzed accordingly. To summarize, the spectral analysis carried out for ZnP−^{3}*PyrF in ZLI is also valid for ZnP−^{3}*PyrF in E-7. In both LCs, ZnP−^{3}*PyrF exhibits similar line shapes attributed mainly to the axial conformer. Thus, the different ratios of ^{3}*ZnP−PyrF/ZnP−^{3}*PyrF in ZLI and E-7 cannot be associated with conformational changes but with the different polarity of these LCs and its effect on the energy levels and, thus, on the electron and energy transfer routes. Contrary to the behavior of covalently linked donor−acceptor systems in different LCs, the polarity of the LC matrix affects the electron transfer process in the ZnP−PyrF complex.[1]

Lending support to the conclusions, derived via the line shape analysis, can be obtained by analyzing the temporal behavior of the magnetization associated with each component of ZnP−PyrF. In Figure 7, we compare the kinetic profiles of $M_y(t)$ of the ^{3}*ZnP−PyrF complex and two control experiments as stated in the figure caption. It is noticeable that the buildup and decay rates of ^{3}*ZnP−PyrF are faster than those of the 1:1 mixture ^{3}*ZnP/C_{60}. Such a behavior is found also in the soft crystalline phase at 220 K (not shown). It is conceivable that the faster decay rates of ^{3}*ZnP−PyrF are due to the additional routes, namely, ET: ^{3}*ZnP−PyrF → ZnP$\bullet^{+-}$PyrF$\bullet^-$ and BET: ZnP$\bullet^{+-}$PyrF$\bullet^-$ → ^{3}*ZnP−PyrF, discussed recently elsewhere.[1]

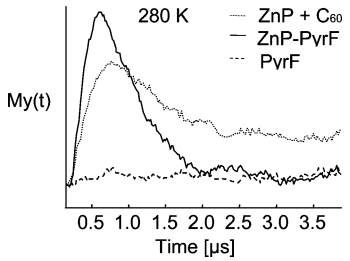

Figure 7. Kinetic profiles, $M_y(t)$, in E-7 at 280 K obtained at 322.5 mT, corresponding to the absorption peak of the ^{3}*ZnP component in the ZnP−PyrF complex and two control experiments: 1:1 mixture of ZnP/C_{60} and the PyrF monomer.

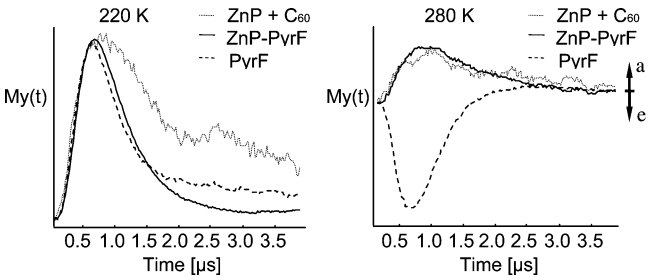

Figure 8. Kinetic profiles, $M_y(t)$, of ^{3}*PyrF in different systems at 335.5 mT (left) and at 335.1 mT (right), at the indicated temperatures. Notice that the absorptive curves are normalized.

Figure 8 shows a comparison between the kinetics of ZnP−^{3}*PyrF, the ^{3}*PyrF monomer, and the control experiment mixture, ZnP/^{3}*C_{60}, at 220 and 280 K. At 220K, $M_y(t)$ of ZnP−^{3}*PyrF decays similarly to that of the ^{3}*PyrF monomer and much faster than the decay of pristine ^{3}*C_{60}. On the other hand, at 280 K at the field where ^{3}*PyrF shows a phase flip, both buildup and decay rates are faster than those of ZnP−^{3}*PyrF and ^{3}*C_{60}. These differences may indicate that the complexation does not allow for dynamics even for the axial configuration. Thus, whereas ^{3}*ZnP−PyrF is characterized by faster rates, indicative of different rates for buildup and decay in the complex and its monomer, no such behavior is observed for ZnP−^{3}*PyrF. It is concluded that the electron transfer processes, which occur in the photoexcited ZnP−PyrF state, involve the ^{3}*ZnP−PyrF moiety but do not affect ZnP−*^{3}PyrF, which is affected only by the singlet−singlet energy transfer occurring at earlier times.[1]

Conclusions

The triplet line shape analysis of PyrF and ZnP−PyrF confirms the routes of ET and EnT processes following photoexcitation in various isotropic and LC environments. Further, the analysis in the LC matrixes enables us to distinguish between different conformations, namely, axial and bent configurations, which occur in the unbound PyrF monomer and to some extent in the ZnP−PyrF complex. The analysis yields that the dominant (85%) axial conformer of unbound ^{3}*PyrF is characterized by triplet parameters obtained in the isotropic solvents and is similar to other monoadducts of C_{60} at similar

experimental conditions. On the other hand, the bent conformer exhibits ZFS parameters of pristine ^{3}*C_{60} at 5 K, with an opposite polarization indicative of either sign reversal of the ZFS parameter, D, or selective population of the Z canonical orientation. It is suggested that the large $|D|$ value as compared to that of ^{3}*C_{60} and its adducts implies localization of the spin density in the poles and, hence, on a sign reversal.

It is concluded that in both LCs, the bound ZnP−PyrF complex mainly exhibits an axial conformation, and thus, the differences between the ET and the EnT routes at each LC are attributed to their different polarity. As was noted,[1] such an effect was in contrast to covalently linked donor−spacer−acceptor systems.

Acknowledgment. The Farkas Center is supported by the Bundesministerium Forschung and Technologie and the Minerva Geselschaft für die Forschung GmbH. This work was supported by the Israel Science Foundation and the Ministry of Science and partially supported by the DFG (H.L.). The work at NYU was supported by grants from the U.S. National Science Foundation. Discussions with Mr. E. Stavitski are highly appreciated.

References and Notes

(1) Galili, T.; Regev, A.; Berg, A.; Levanon, H.; Schuster, D. I.; Möbius, K.; Savitsky, A. *J. Phys. Chem. A* **2005**, *109*, 8451.
(2) Prato, M.; Maggini, M. *Acc. Chem. Res.* **1998**, *31*, 519.
(3) Guldi, D. M.; Prato, M. *Acc. Chem. Res.* **2000**, *33*, 695.
(4) Guldi, D. M.; Martin, N. *J. Mater. Chem.* **2002**, *12*, 1978.
(5) Bosi, S.; Da Ros, T.; Spalluto, G.; Prato, M. *Eur. J. Med. Chem.* **2003**, *38*, 913.
(6) Bracher, P. J.; Schuster, D. I. Electron Transfer in Functionalized Fullerenes. In *Fullerenes: From Synthesis to Optoelectronic Applications*; Guldi, D. M., Martin, N., Eds.; Kluwer Academic Publishers: Dordrecht, The Netherlands, 2002; p 163.
(7) Ward, M. D. *Chem. Soc. Rev.* **1997**, *26*, 365.
(8) D'Souza, F.; Deviprasad, G. R.; Rahman, M. S.; Choi, J. P. *Inorg. Chem.* **1999**, *38*, 2157.
(9) Da Ros, T.; Prato, M.; Guldi, D.; Alessio, E.; Ruzzi, M.; Pasimeni, L. *Chem. Commun.* **1999**, 635.
(10) Da Ros, T.; Prato, M.; Guldi, D. M.; Ruzzi, M.; Pasimeni, L. *Chem.−Eur. J.* **2001**, *7*, 816.
(11) Guldi, D. M.; Luo, C. P.; Da Ros, T.; Prato, M.; Dietel, E.; Hirsch, A. *Chem. Commun.* **2000**, 375.
(12) D'Souza, F.; Deviprasad, G. R.; Zandler, M. E.; Hoang, V. T.; Klykov, A.; VanStipdonk, M.; Perera, A.; El-Khouly, M. E.; Fujitsuka, M.; Ito, O. *J. Phys. Chem. A* **2002**, *106*, 3243.
(13) Tat, F. T.; Zhou, Z. G.; MacMahon, S.; Song, F. Y.; Rheingold, A. L.; Echegoyen, L.; Schuster, D. I.; Wilson, S. R. *J. Org. Chem.* **2004**, *69*, 4602.
(14) Berg, A.; Galili, T.; Levanon, H.; Kotlyar, A. B.; Hazani, M. *J. Phys. Chem. A* **1999**, *103*, 8372.
(15) Honeywell, B. J. http://www.bandj.com/BJSolvents, 2004.
(16) Merck, E. *Merck Ltd. Catalog: Nematic Liquid Crystal Mixtures*, 1989.
(17) Gonen, O.; Levanon, H. *J. Chem. Phys.* **1986**, *84*, 4132.
(18) Sun, Y.-P. *Photoexcited States and Charge-Transfer Properties of Fullerene Materials; Fullerenes. Recent advances in the chemistry and physics of fullerenes and related material*; Reno, NV, 1995.
(19) Levanon, H.; Hasharoni, K. *Prog. React. Kinet.* **1995**, *20*, 309.
(20) Regev, A.; Galili, T.; Levanon, H. *J. Phys. Chem.* **1996**, *100*, 18502.
(21) Wilson, S. R.; MacMahon, S.; Tat, F. T.; Jarowski, P. D.; Schuster, D. I. *Chem. Commun.* **2003**, 226.
(22) Wasielewski, M. R.; O'Neil, M. P.; Lykke, K. R.; Pellin, M. J.; Gruen, D. M. *J. Am. Chem. Soc.* **1991**, *113*, 2774.
(23) Levanon, H.; Meiklyar, V.; Michaeli, A.; Michaeli, S.; Regev, A. *J. Phys. Chem.* **1992**, *96*, 6128.
(24) Levanon, H.; Meiklyar, V.; Michaeli, S.; Gamliel, D. *J. Am. Chem. Soc.* **1993**, *115*, 8722.
(25) Regev, A.; Gamliel, D.; Meiklyar, V.; Michaeli, S.; Levanon, H. *J. Phys. Chem.* **1993**, *97*, 3671.
(26) Levanon, H.; Michaeli, S.; Meiklyar, V. *Triplet dynamics of C_{60} and C_{70} and its participation in electron transfer reactions. Time-resolved electron paramagnetic resonance*; The Electrochemical Society: Pennington, NJ, 1994; Vol. 1.
(27) Bennati, M.; Grupp, A.; Mehring, M. *J. Chem. Phys.* **1995**, *102*, 9457.
(28) Galili, T.; Regev, A.; Levanon, H.; Schuster, D. I.; Guldi, D. M. *J. Phys. Chem. A* **2004**, *108*, 10632.
(29) Surjan, P. R.; Nemeth, K.; Bennati, M.; Grupp, A.; Mehring, M. *Chem. Phys. Lett.* **1996**, *251*, 115.
(30) van den Berg, G. J. B.; van den Heuvel, D. J.; Poluektov, O. G.; Holleman, I.; Groenen, E. J. J. *J. Magn. Reson.* **1998**, *131*, 39.
(31) Dauw, X. L. R.; van den Berg, G. J. B.; van den Heuvel, D. J.; Poluektov, O. G.; Groenen, E. J. J. *J. Chem. Phys.* **2000**, *112*, 7102.
(32) Kallay, M.; Nemeth, K.; Surjan, P. R. *J. Phys. Chem. A* **1998**, *102*, 1261.
(33) Visser, J.; Groenen, E. J. J. *Chem. Phys. Lett.* **2002**, *356*, 43.
(34) Bennati, M.; Grupp, A.; Mehring, M.; Belik, P.; Gugel, A.; Mullen, K. *Chem. Phys. Lett.* **1995**, *240*, 622.
(35) Agostini, G.; Corvaja, C.; Pasimeni, L. *Chem. Phys.* **1996**, *202*, 349.
(36) Pasimeni, L.; Hirsch, A.; Lamparth, I.; Herzog, A.; Maggini, M.; Prato, M.; Corvaja, C.; Scorrano, G. *J. Am. Chem. Soc.* **1997**, *119*, 12896.
(37) Pasimeni, L.; Segre, U.; Ruzzi, M.; Maggini, M.; Prato, M.; Kordatos, K. *J. Phys. Chem. B* **1999**, *103*, 11275.
(38) Bortolus, M.; Prato, M.; van Tol, J.; Maniero, A. L. *Chem. Phys. Lett.* **2004**, *398*, 228.
(39) Yamauchi, S.; Funayama, T.; Ohba, Y.; Paul, P.; Reed, C. A.; Fujiwara, K.; Komatsu, K. *Chem. Phys. Lett.* **2002**, *363*, 199.
(40) Corvaja, C.; Maggini, M.; Ruzzi, M.; Scorrano, G.; Taffoletti, A. *Appl. Magn. Reson.* **1997**, *12*, 477.
(41) Mizuochi, N.; Ohba, Y.; Yamauchi, S. *J. Chem. Phys.* **1999**, *111*, 3479.
(42) Brustolon, M.; Zoleo, A.; Agostini, G.; Maggini, M. *J. Phys. Chem. A* **1998**, *102*, 6331.
(43) Zoleo, A.; Maniero, A. L.; Prato, M.; Severin, M. G.; Brunel, L. C.; Kordatos, K.; Brustolon, M. *J. Phys. Chem. A* **2000**, *104*, 9853.
(44) Conti, F.; Corvaja, C.; Maggini, M.; Scorrano, G.; Ceroni, P.; Paolucci, F.; Roffia, S. *Phys. Chem. Chem. Phys.* **2001**, *3*, 3518.
(45) Zoleo, A.; Maniero, A. L.; Bellinazzi, M.; Prato, M.; Da Ros, T.; Brunel, L. C.; Brustolon, M. *J. Magn. Reson.* **2002**, *159*, 226.
(46) Agostini, G.; Corvaja, C.; Maggini, M.; Pasimeni, P.; Prato, M. *J. Phys. Chem.* **1996**, *100*, 13416.
(47) Agostini, G.; Pasimeni, L.; Ruzzi, M.; Monti, S.; Maggini, M.; Prato, M.; Lamparth, I.; Hirsch, A. *Chem. Phys.* **2000**, *253*, 105.
(48) Knorr, S.; Grupp, A.; Mehring, M.; Grube, G.; Effenberger, F. *J. Chem. Phys.* **1999**, *110*, 3502.